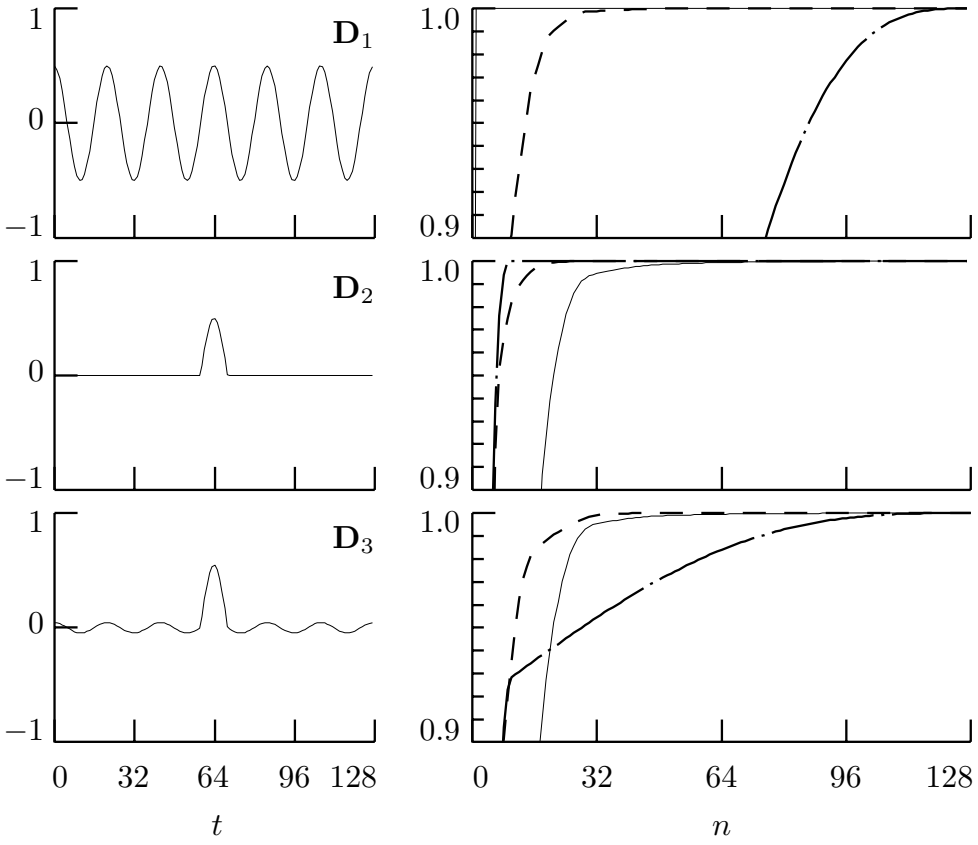

Figure 396. Three signals (left-hand column) and their corresponding normalized partial energy sequences (right-hand column) for the signals themselves (curves broken by intermittent dots), their ODFT coefficients (thin solid curves) and their LA(8) DWT coefficients (dashed curves).

	domain of signal		
	frequency	time	mixture
$\mathcal{F}$	2	29	28
I_N	105	9	75
$\mathcal{W}$	22	14	21

Table 396. Number of coefficients required to obtain no more than a 1% relative approximation error for three signals using an orthonormal discrete Fourier transform $\mathcal{F}$, an identity transform I_N and an LA(8) DWT transform $\mathcal{W}$ (see text for details).

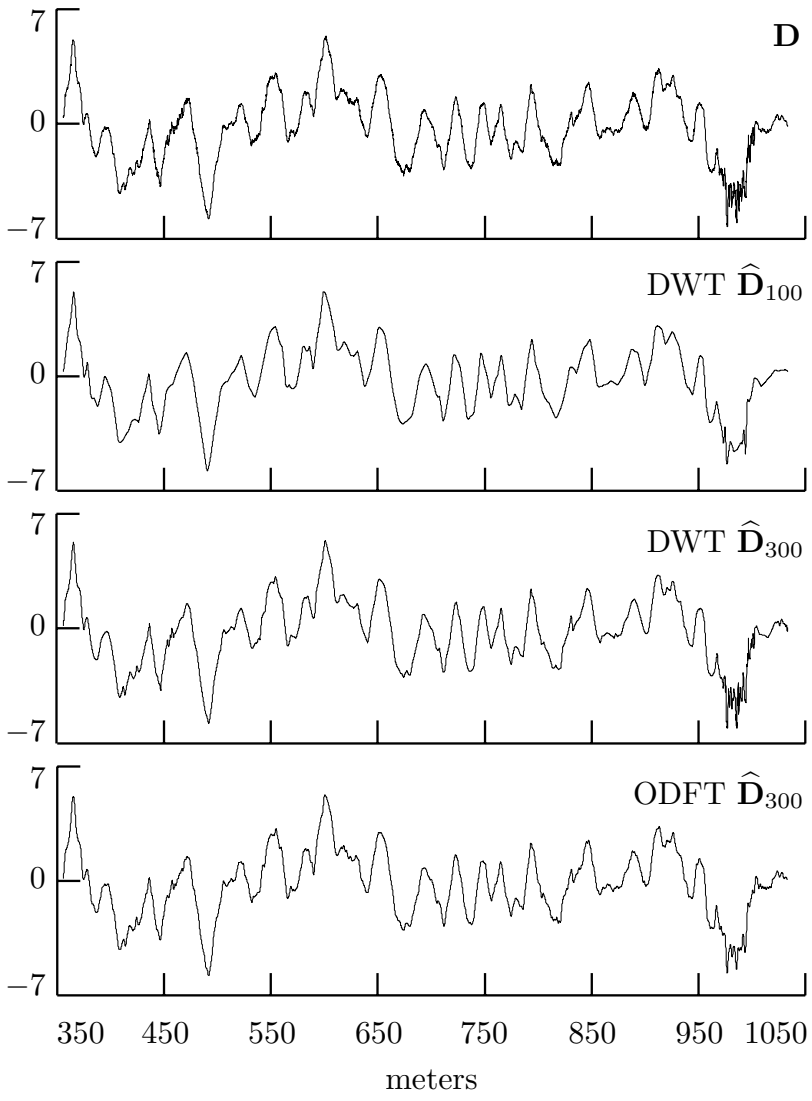

Figure 397. Plot of $N = 6784$ values of a hypothesized signal $\mathbf{D}$ related to vertical shear in the ocean versus depth in meters (top plot), along with reconstructions using 100 LA(8) DWT coefficients, 300 LA(8) DWT coefficients and 300 ODFT coefficients. See Section 5.10 for more discussion about these data.

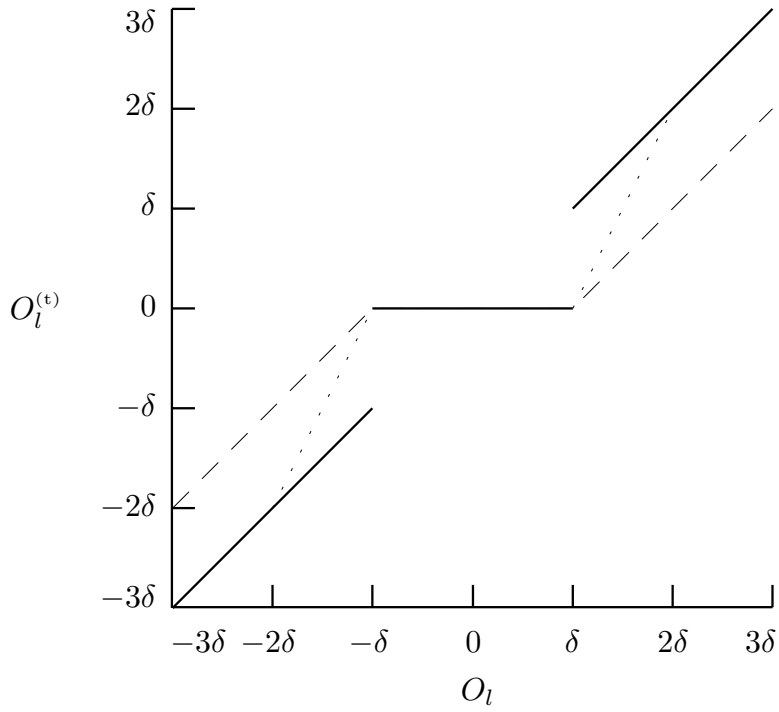

Figure 399. Mappings from O_l to $O_l^{(\mathrm{t})}$, where $O_l^{(\mathrm{t})}$ is either $O_l^{(\mathrm{ht})}$ for hard thresholding (solid lines), $O_l^{(\mathrm{st})}$ for soft thresholding (dashed lines), or $O_l^{(\mathrm{mt})}$ for mid thresholding (dotted lines). Note that the effect of all three thresholding schemes is the same when $-\delta \leq O_l \leq \delta$.

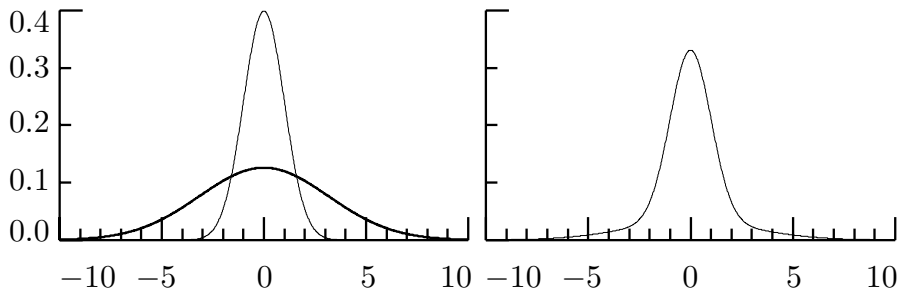

Figure 410. PDFs for $\mathcal{N}(0,1)$ and $\mathcal{N}(0,10)$ RVs (left-hand plot, thin and thick curves, respectively) and for an RV obeying a Gaussian mixture model (right-hand plot). The mixture PDF is non-Gaussian and is formed by adding the $\mathcal{N}(0,1)$ and $\mathcal{N}(0,10)$ PDFs, weighted by $p_l = 0.75$ and $1 - p_l = 0.25$, respectively (adapted from Figure 1 of Chipman *et al.*, 1997).

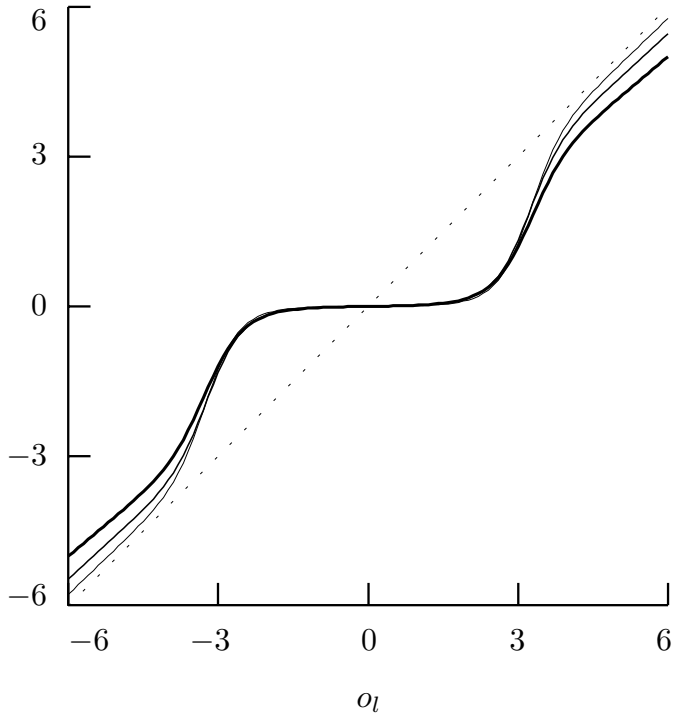

Figure 412. The conditional mean shrinkage rule of Equation (411c) for $p_l = 0.95, \sigma^2_{n_l} = 1$ and $\sigma^2_{G_l} = 5$ (thickest curve, furthest from dotted diagonal), 10 and 25 (thinnest curve, nearest to diagonal). Because of the correspondence between conditional mean shrinkage rules and the Bayes rule estimators of Chipman *et al.* (1997) with respect to squared error loss, the above also illustrates $B_2(\cdot)$ of Equation (414a).

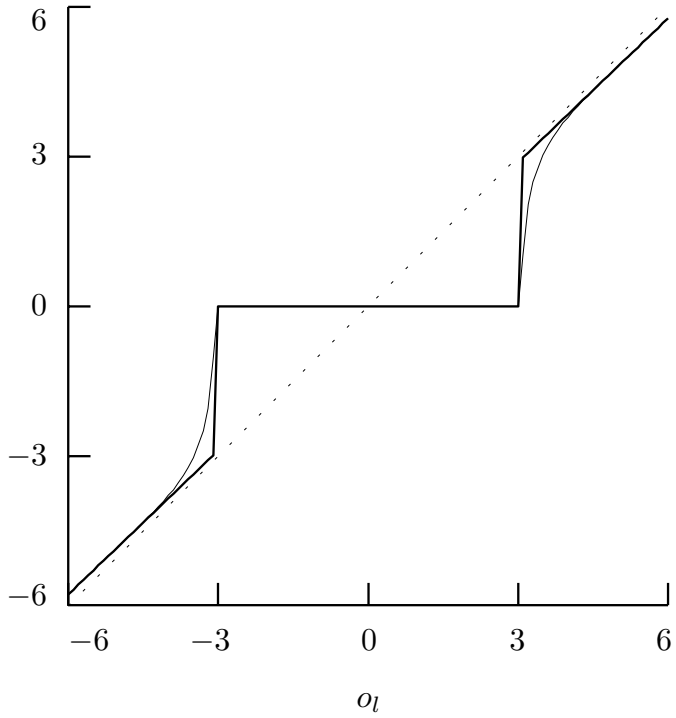

Figure 416. Comparison of the posterior median $B_1(o_l)$ (thin curve) to the *approximate* conditional median $U_1(o_l)$ (thick) when $\sigma^2_{G_l} = 25, p_l = 0.95$ and $\sigma^2_{n_l} = 1$. The dotted line marks the diagonal.

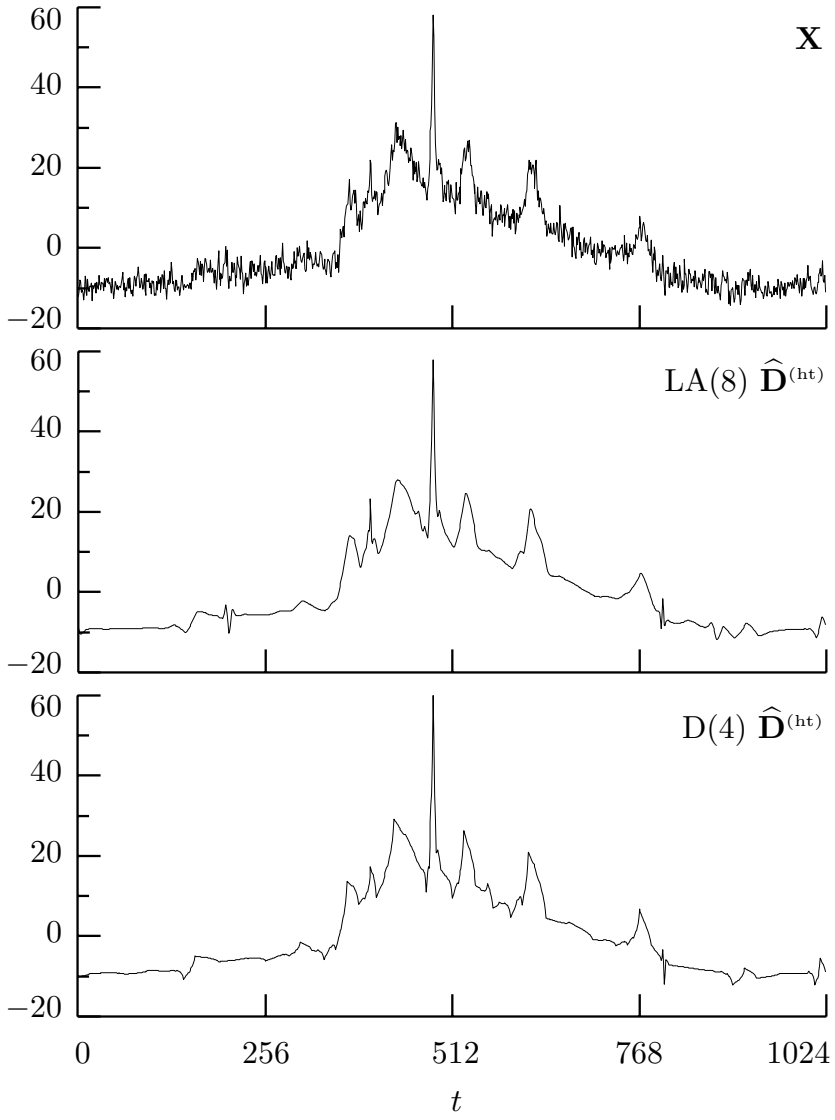

Figure 418. Nuclear magnetic resonance (NMR) spectrum (top plot), along with wavelet-based hard threshold signal estimates using the level $J_0 = 6$ partial LA(8) DWT (middle) and a similar D(4) DWT (bottom). In both cases, we determine the noise variance σ_ϵ^2 using the MAD standard deviation estimate $\hat{\sigma}_{(\mathrm{mad})}$, after which we set the universal threshold level $\hat{\delta}^{(\mathrm{u})} \equiv \sqrt{[2\hat{\sigma}^2_{(\mathrm{mad})} \log(N)]}$. This NMR spectrum was extracted from the public domain software package `WaveLab`, to which it was provided by Andrew Maudsley, Department of Radiology, University of California, San Francisco (the data can be accessed via the Web site for this book – see page *xiv*).

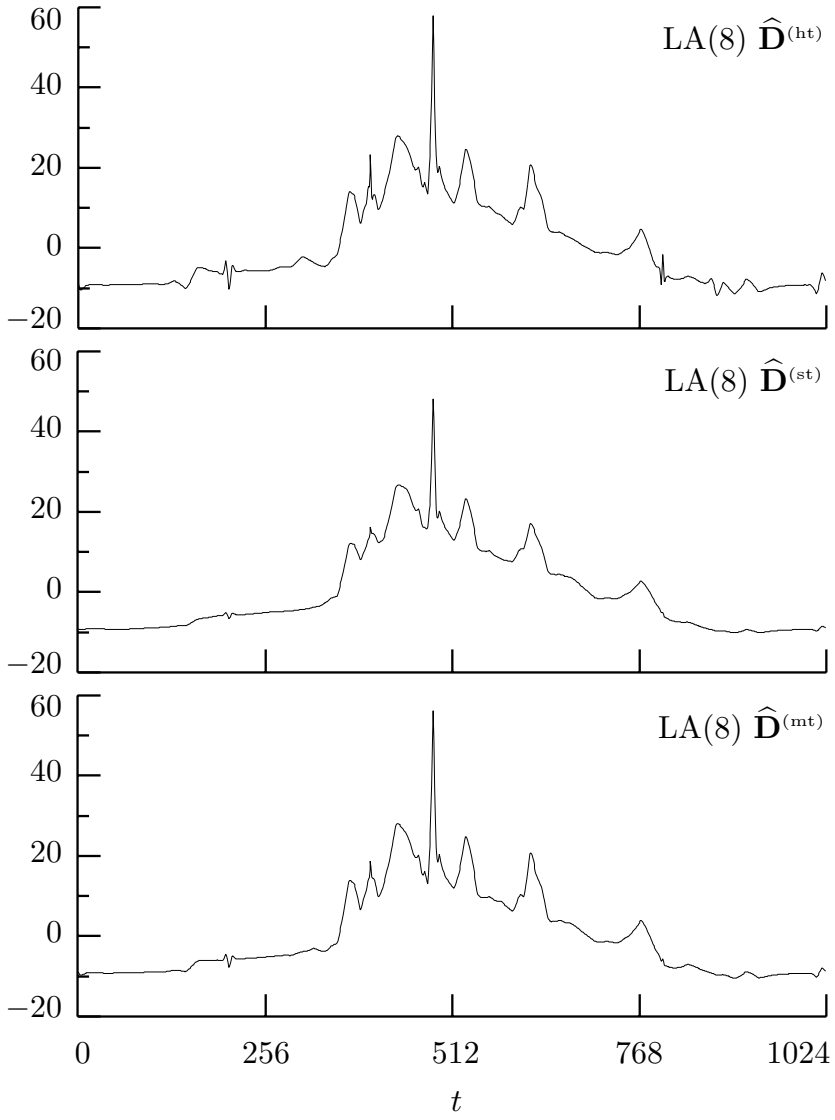

Figure 419. Thresholding signal estimates of the NMR spectrum based upon the level $J_0 = 6$ partial LA(8) DWT with – from top to bottom – hard, soft and mid thresholding (the top plot is a repeat of the middle of Figure 418). For all three estimates, we use the universal threshold level $\hat{\delta}^{(\mathrm{u})} \equiv \sqrt{[2\hat{\sigma}^2_{(\mathrm{mad})} \log(N)]} \doteq 6.12622$ based upon the MAD standard deviation estimate $\hat{\sigma}_{(\mathrm{mad})} \doteq 1.64538$.

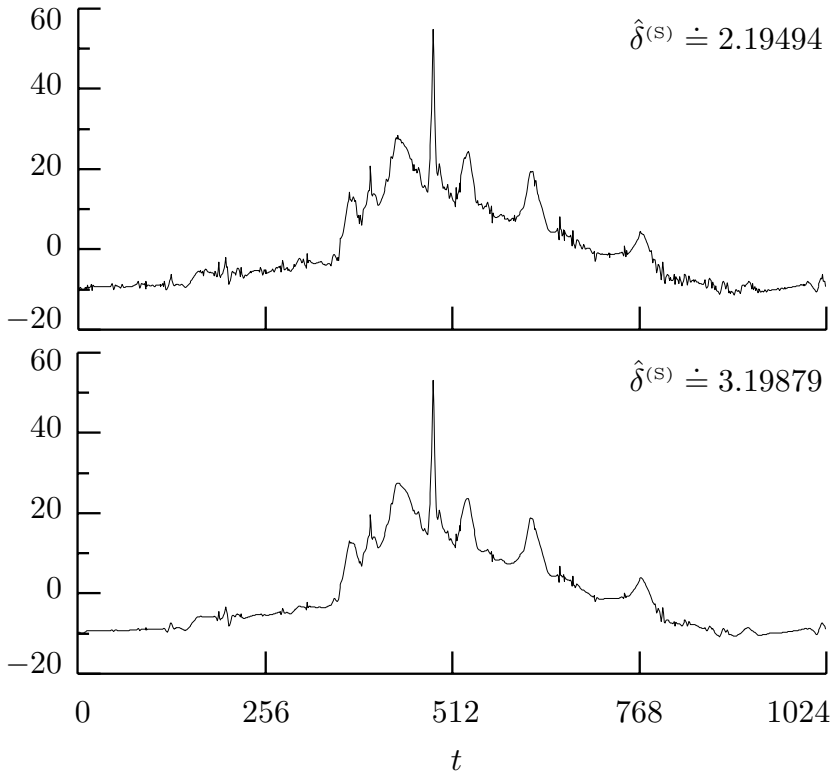

Figure 421. Thresholding signal estimates of the NMR spectrum based upon the level $J_0 = 6$ partial LA(8) DWT with soft thresholding and SURE threshold levels $\hat{\delta}^{(S)}$, which are computed using MAD scale estimates based on, respectively, just the unit scale wavelet coefficients (top plot) and wavelet coefficients from all six scales (bottom).

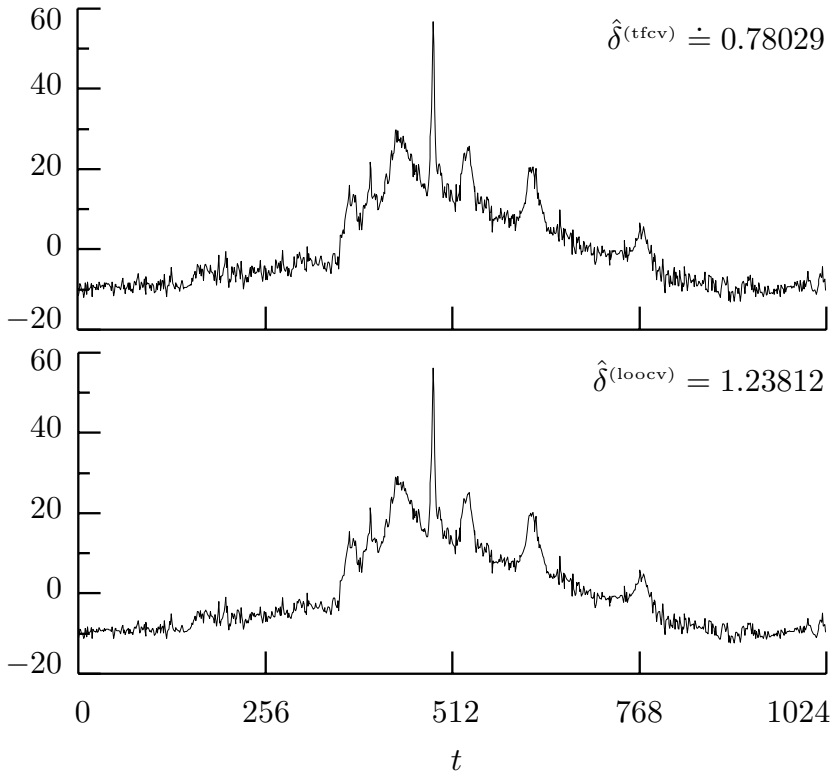

Figure 423. Thresholding signal estimates of the NMR spectrum based upon the level $J_0 = 6$ partial LA(8) DWT with soft thresholding and threshold levels determined by two-fold cross-validation (top plot) and leave-one-out cross-validation (bottom).

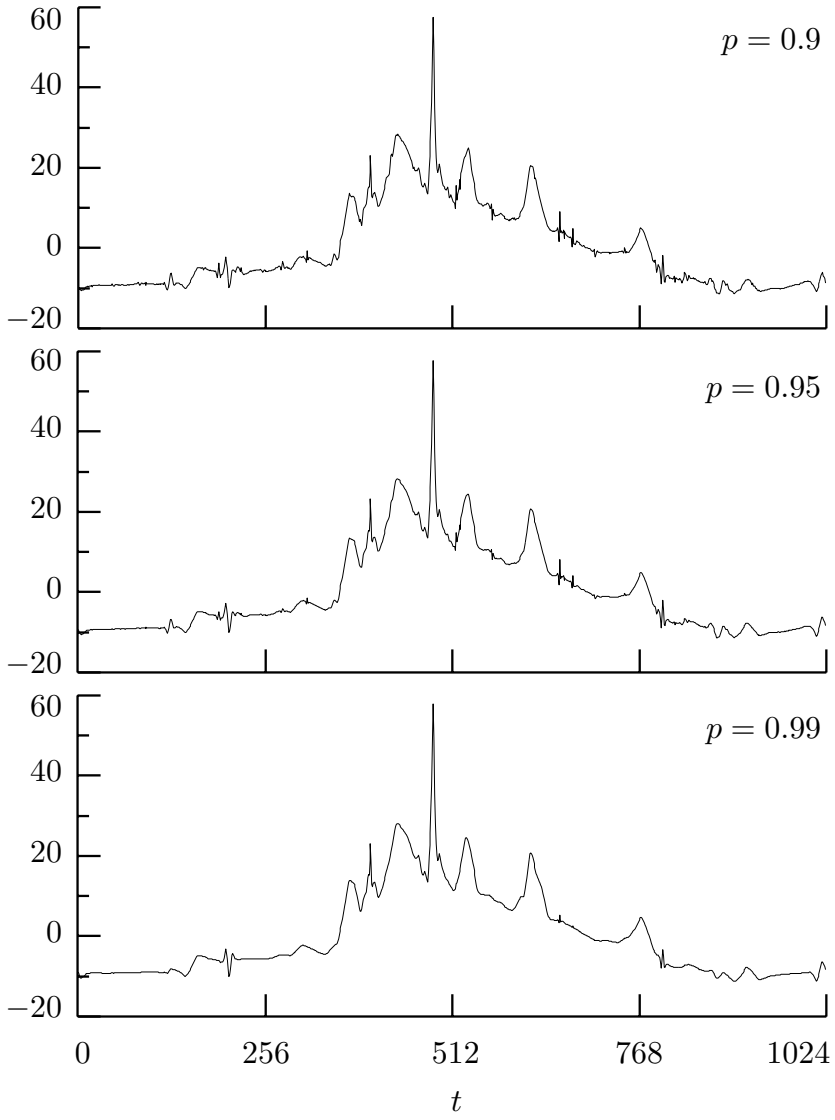

Figure 425. Shrinkage signal estimates of the NMR spectrum based upon the level $J_0 = 6$ partial LA(8) wavelet transform and the conditional mean with $p = 0.9$ (top plot), 0.95 (middle) and 0.99 (bottom). The remaining parameters (namely, σ^2_ϵ, σ^2_W and σ^2_G) are estimated as explained in the text.

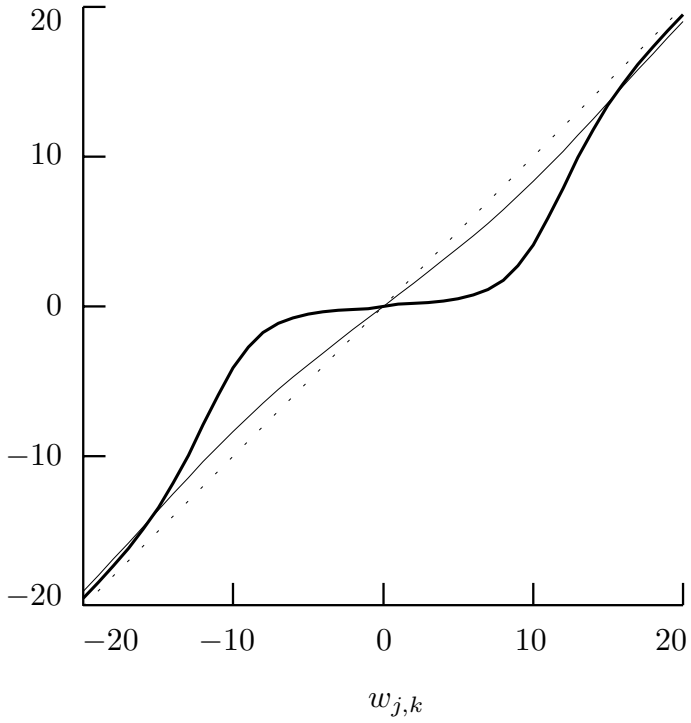

Figure 427. Bayes rules $B_2(w_{j,k})$ versus $w_{j,k}$ for the Vidakovic (1998) scheme as applied to the NMR spectrum. The thin and thick curves depict $B_2(\cdot)$ assuming degrees of freedom ϑ of, respectively, 5 and 2.01. The dotted line marks the diagonal. The corresponding signal estimates are shown in Figure 428.

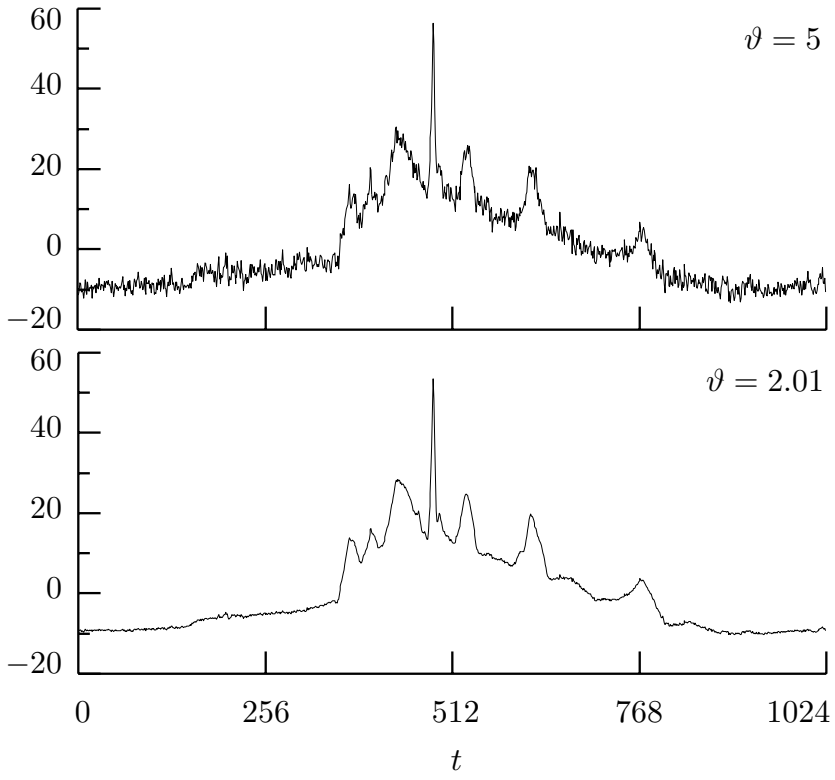

Figure 428. Shrinkage signal estimates of the NMR spectrum based upon the level $J_0 = 6$ partial LA(8) wavelet transform and the Bayes rule $B_2(\cdot)$ as formulated by Vidakovic (1998) and given in Equation (414b) (the specific rule for each estimate is plotted in Figure 427). The difference between the two estimates is solely due to the choice of the degrees of freedom ϑ for the signal PDF $f_R(\cdot)$, with the remaining two parameters (κ and υ) estimated as described in the text.

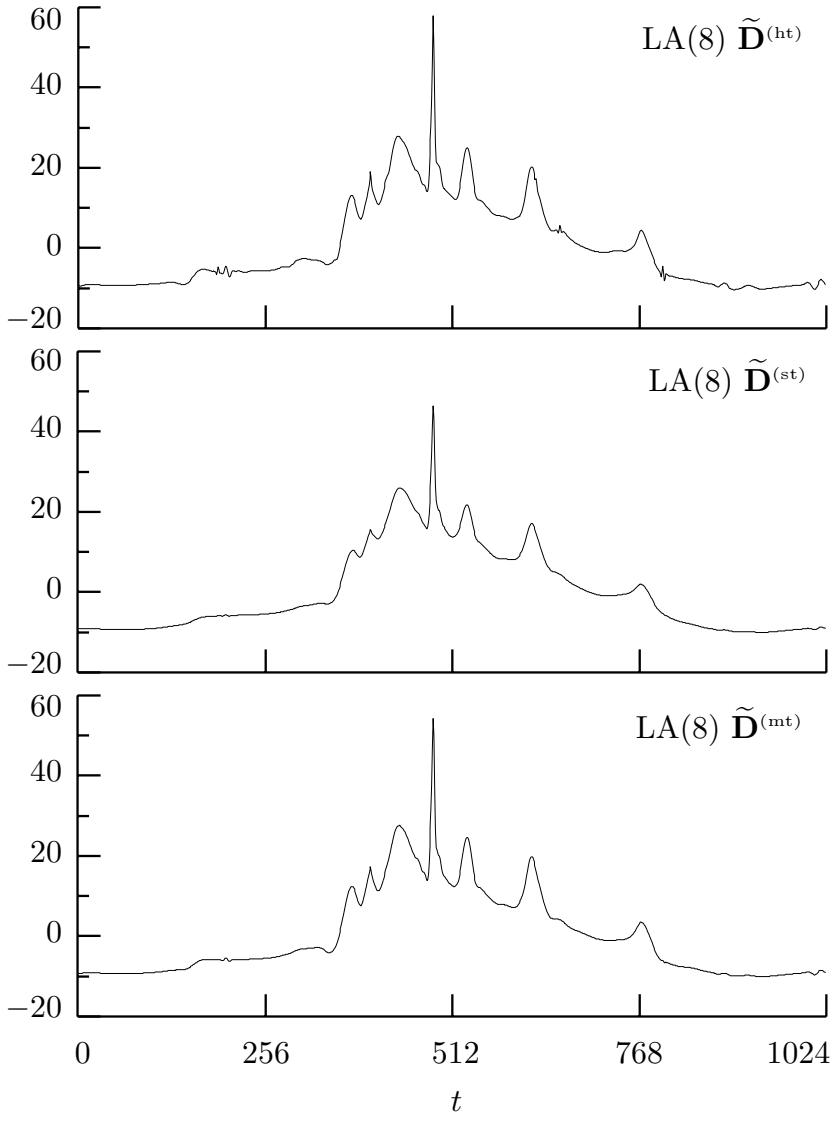

Figure 430. Thresholding signal estimates of the NMR spectrum based upon the level $J_0 = 6$ LA(8) MODWT with – from top to bottom – hard, soft and mid thresholding (Figure 419 has corresponding plots for the DWT). Each estimate uses the universal threshold levels $\tilde{\delta}_j^{(\mathrm{u})} \equiv \sqrt{[2\tilde{\sigma}^2_{(\mathrm{mad})} \log(N)/2^j]} \doteq 6.49673/2^{j/2}$ computed via the MODWT-based MAD standard deviation estimate $\tilde{\sigma}_{(\mathrm{mad})} \doteq 1.74489$.

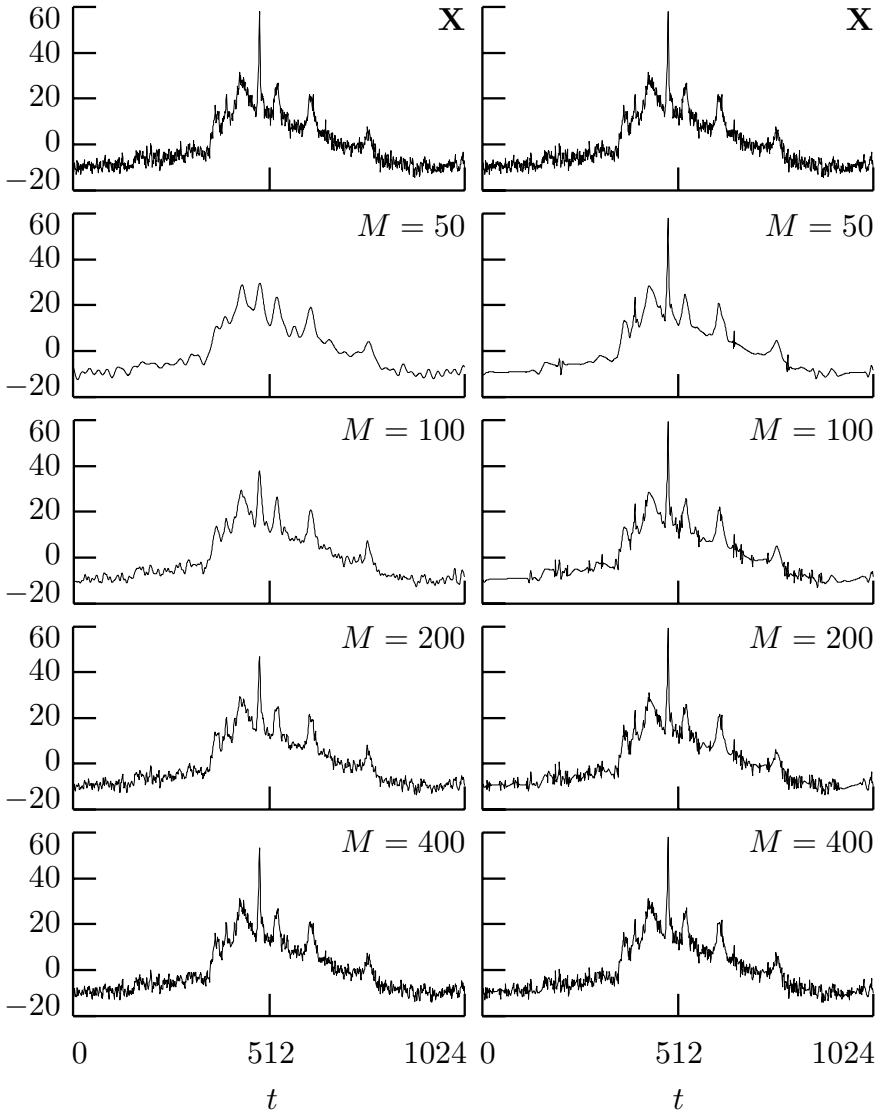

Figure 431. Denoising of NMR spectrum (top plot) using hard thresholding based upon keeping the M coefficients with the largest magnitudes in the ODFT (left-hand column) and the level $J_0 = 6$ partial LA(8) DWT (right-hand) for $M = 50$, 100, 200 and 400 (second to fifth rows, respectively).

	j							
	1	2	3	4	5	6	7	8
$-\delta^{(\mathrm{l})}_{j,\frac{\alpha}{2}}$	7.825	7.031	6.228	5.750	5.460	5.287	5.182	5.118
$\delta^{(\mathrm{u})}_{j,\frac{\alpha}{2}}$	5.556	5.601	5.142	4.976	4.913	4.901	4.910	4.925

Table 436. Lower and upper thresholds $\delta^{(\mathrm{l})}_{j,\frac{\alpha}{2}}$ and $\delta^{(\mathrm{u})}_{j,\frac{\alpha}{2}}$, $j = 1, \ldots, 8$, for wavelet-based thresholding of the log periodogram using the LA(8) DWT. Here we use the approximation $\alpha = P_F/M$ with $P_F = 0.1$ and $M = 1024$. For convenience, we have tabulated $-\delta^{(\mathrm{l})}_{j,\frac{\alpha}{2}}$ instead of $\delta^{(\mathrm{l})}_{j,\frac{\alpha}{2}}$. Note that, as j increases, the lower and upper thresholds come closer to each other in magnitude, as would be expected due to convergence to Gaussianity.

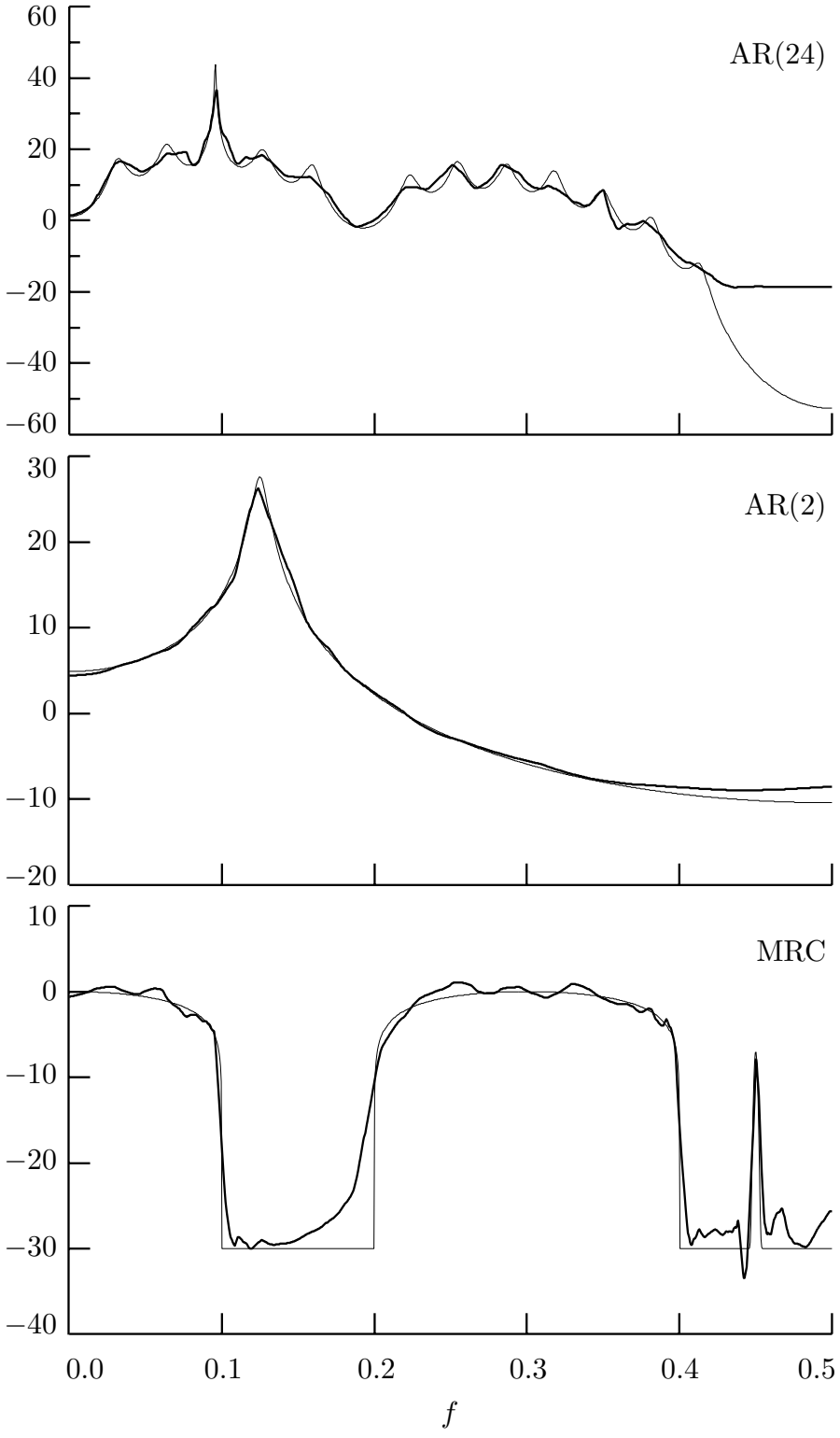

Figure 438. Periodogram-based estimated SDFs (thick curves) and true SDFs (thin) for the AR(24), AR(2) and MRC processes (see the text for details).

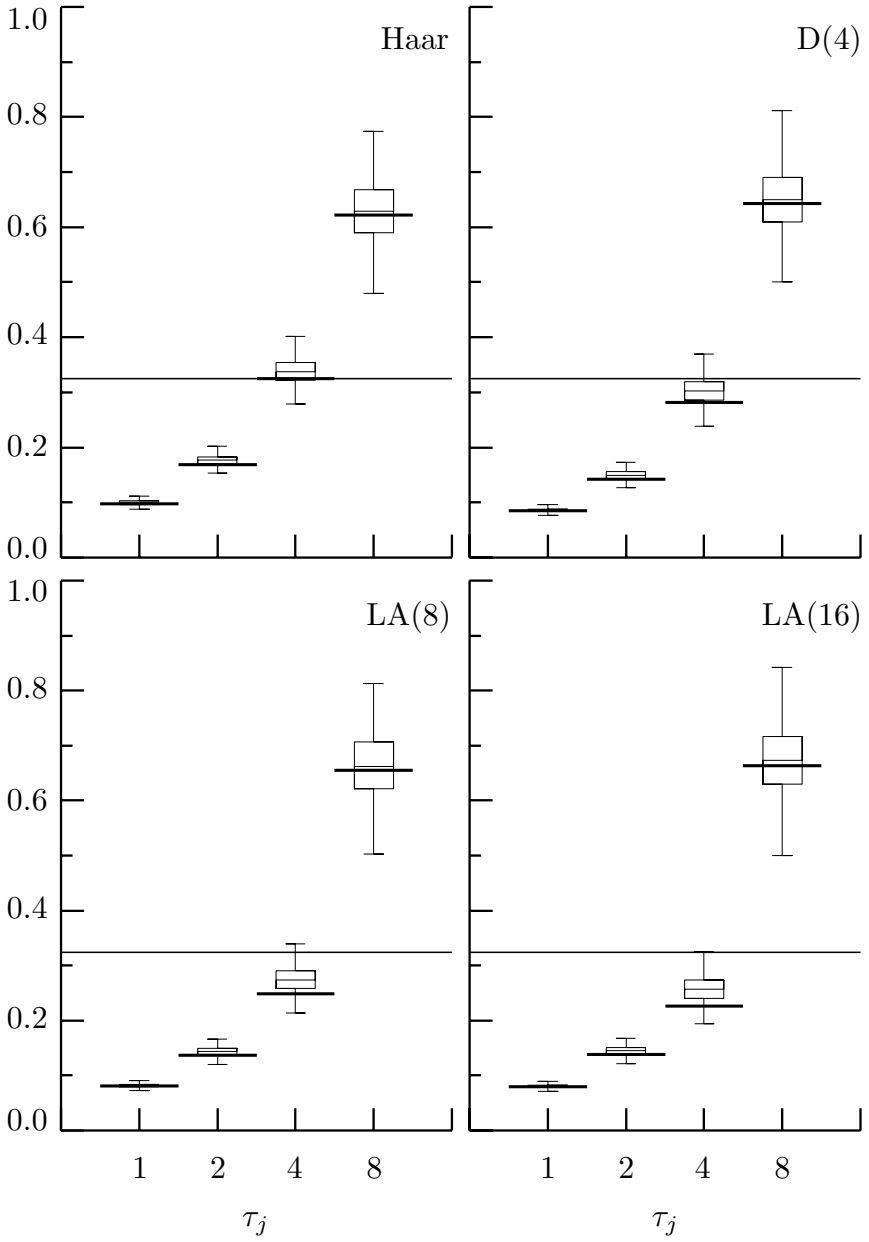

Figure 443. Box plots of the estimated standard deviations $\hat{\sigma}_j$ of wavelet coefficients $n_{j,t}$ at levels $j = 1, 2, 3$ and 4 derived from the AR(2) process using different wavelet filters, for $N = 2048$ and $K = 10$. The horizontal solid lines extending beyond each box plot indicate the value of σ_j derived from Equation (441b). The 'nominal' standard deviation $\sigma_\eta = \sqrt{[\psi'(10)]} \doteq 0.32$ is marked as a solid horizontal line right across each of the plots.

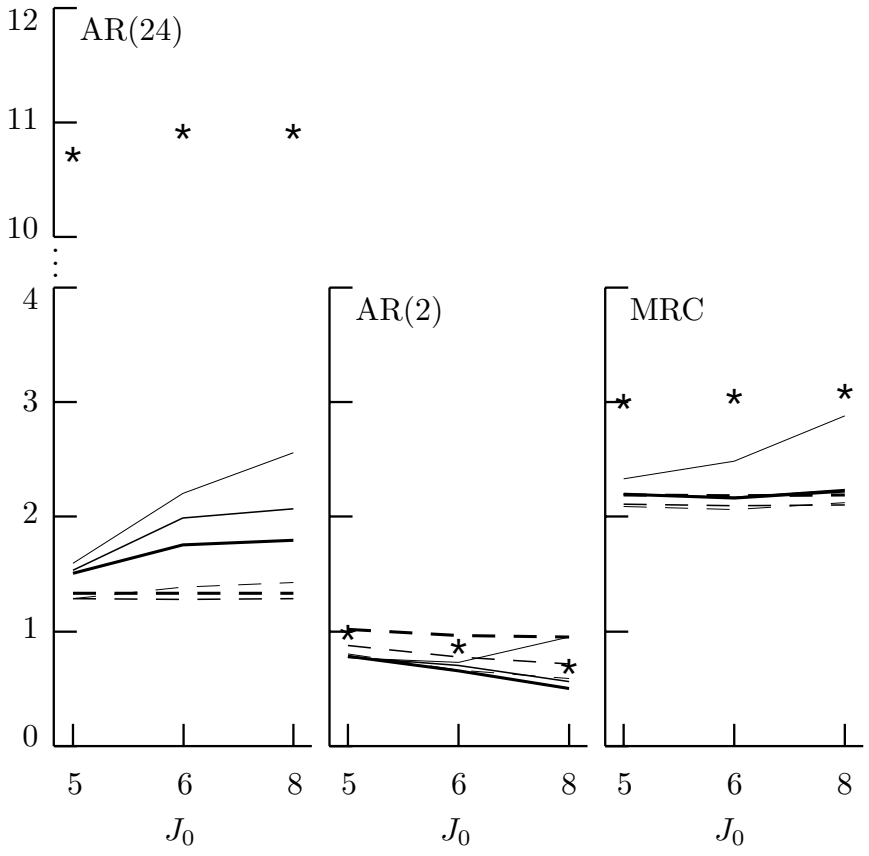

Figure 446. Average value over a thousand simulations of the RMSEs for the AR(24) (left-hand plot), AR(2) (center) and MRC models (right-hand). In each plot, the average RMSE (in dBs) is plotted for the level-dependent multitaper-based method with hard (solid thick curve), mid (solid medium) and soft (solid thin) thresholding and also for the level-independent method with hard (dashed thick curve), mid (dashed medium) and soft (dashed thin) thresholding. Three values of level J_0 are considered, namely 5, 6 and 8, corresponding to 64, 32 and 8 scaling coefficients left untouched by the thresholding. The asterisks show average RMSEs for the periodogram-based method. In all cases, the series length is $N = 2048$, and we use the LA(8) wavelet to compute the DWT.

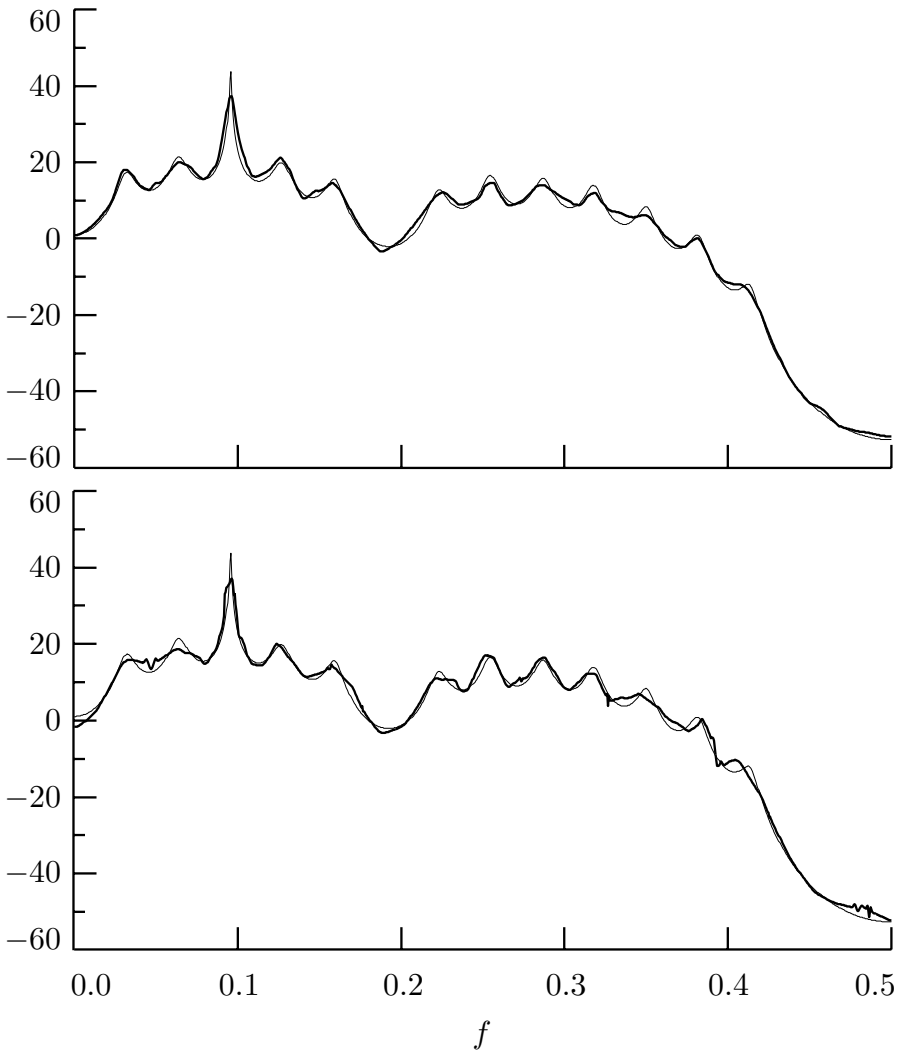

Figure 447. Estimated SDFs (thick curves) and true SDF (thin) for the AR(24) process. The SDF estimates are representative in that they have RMSEs closest to the average RMSE over a thousand simulations. The upper plot is for level-independent soft thresholding, and the lower plot, level-dependent hard thresholding, with $J_0 = 5$ in both cases. The simulated series are of length $N = 2048$, and we use an LA(8) DWT.

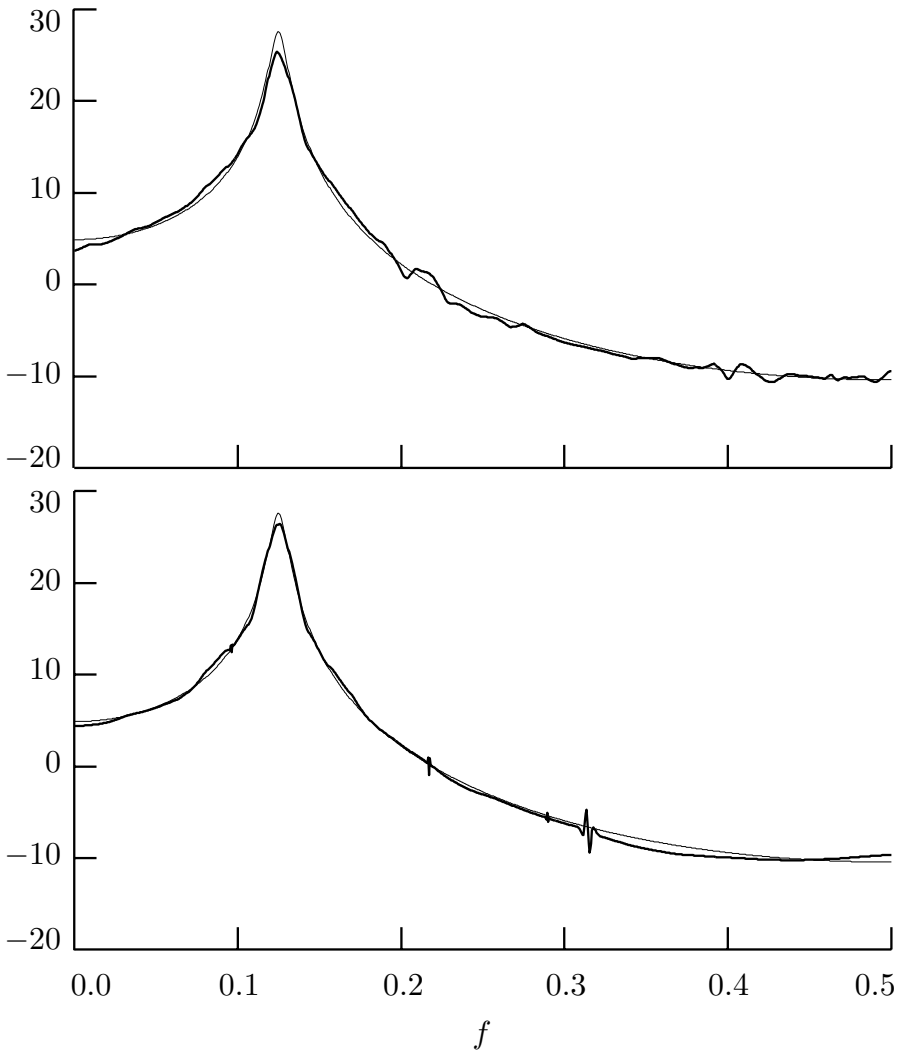

Figure 448. Estimated SDFs (thick curves) and true SDF (thin) for the AR(2) process. Layout and parameters are as for Figure 447.

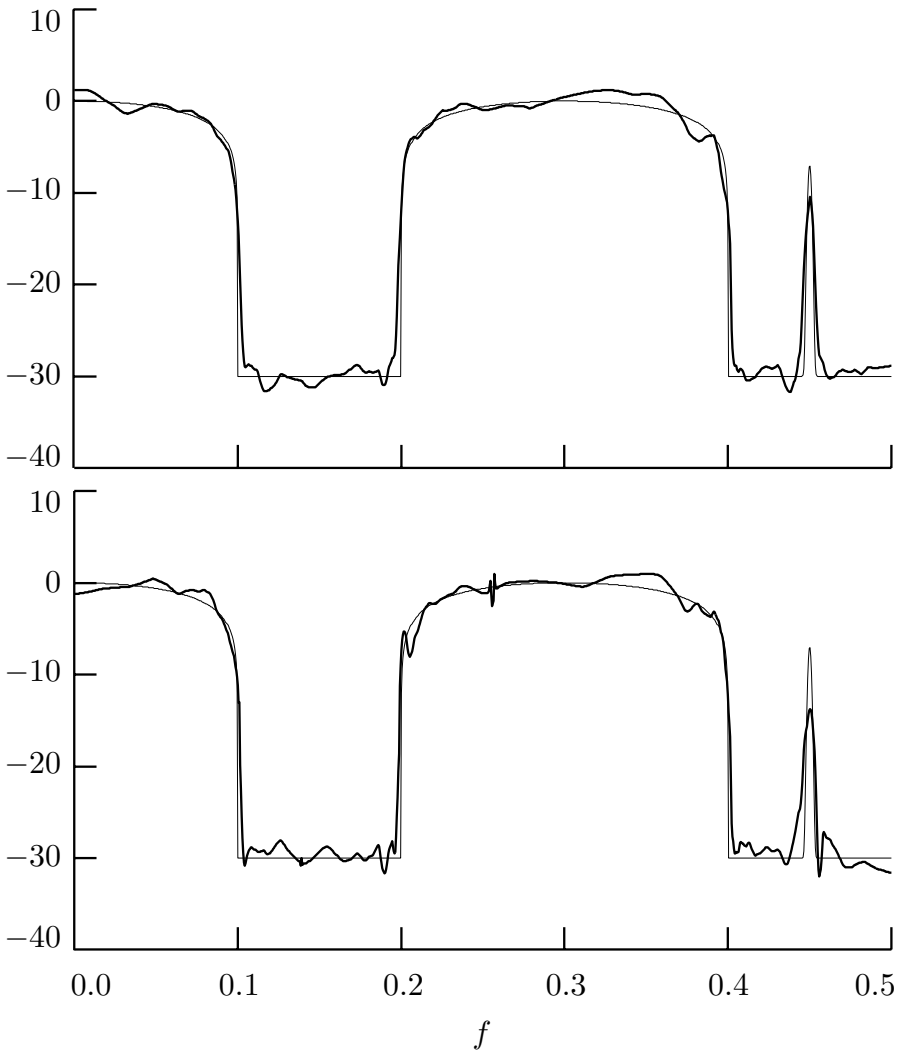

Figure 449. Estimated SDF (thick curve) and true SDF (thin curve) for the mobile radio communications process. Layout and parameters are as for Figure 447.